Electronic Supplementary Material (ESI) for Chemical Science

Water in the Earth's Mantle: A Solid-State NMR Study of Hydrous Wadsleyite

John M. Griffin, Andrew J. Berry, Daniel J. Frost, Stephen Wimperis,

and Sharon E. Ashbrook

Supporting Information

S1. FTIR spectra of hydrous wadsleyite

Figure S1.1 shows the unpolarised FTIR spectrum of wads-D.

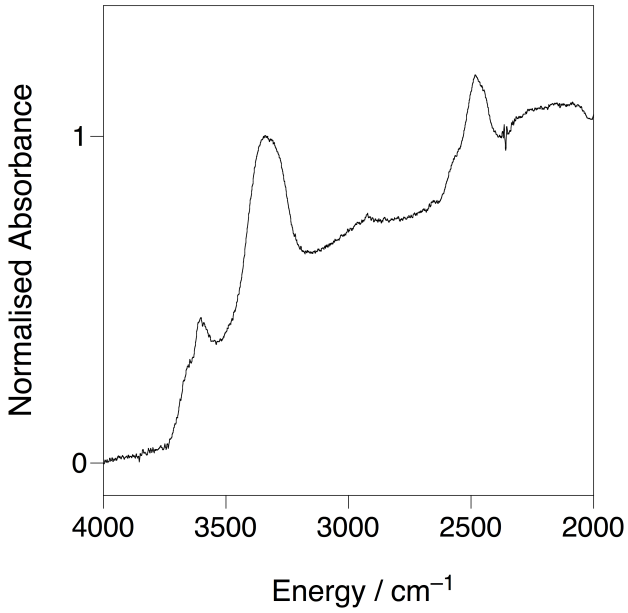

Figure S1.1 Normalised, unpolarised FTIR spectra of the O-H stretching region of hydrous wadsleyite containing $^{1}H/^{2}H$.

S2. Comparison of ^{17}O MQMAS and STMAS NMR spectra for wads-H

A triple-quantum (TQ) MAS NMR spectrum was recorded for wads-H using a phase-modulated split-t_1 shifted echo pulse sequence. In Figure S2.1, the TQMAS NMR spectrum is compared with the ^{17}O STMAS NMR spectrum of the same sample shown in Figure 2d in the main text. The two spectra are almost identical in appearance, although the TQMAS NMR spectrum exhibits lower signal-to-noise (especially for the hydroxyl oxygen resonance) owing to the lower sensitivity of this approach. This indicates that the observed broadening in the δ_1 and δ_2 dimensions results from disorder, rather than dynamic processes.

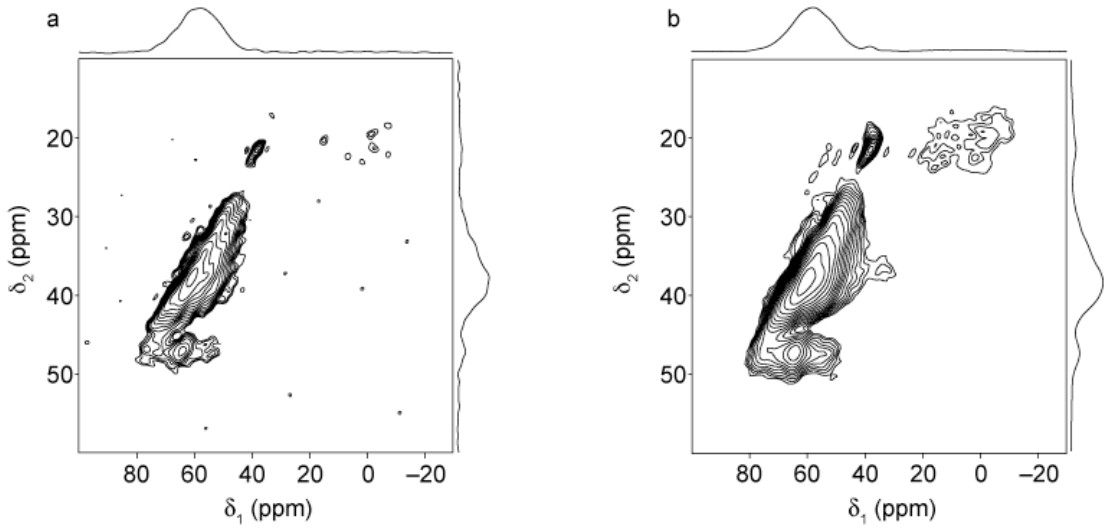

Figure S2.1 (a) ^{17}O (20.0 T) TQMAS and (b) STMAS NMR spectra of wads-H. The TQMAS NMR spectrum is the result of coadding 864 transients separated by a recycle interval of 1 s, for each of the 64 t_1 increments of 86.1 μs. An echo interval of 1.8 ms was used.

S3. Local coordination environments in wadsleyite

Figure S3.1 shows the local coordination environments for each oxygen, silicon and magnesium species in the crystal structure of anhydrous wadsleyite.[S1]

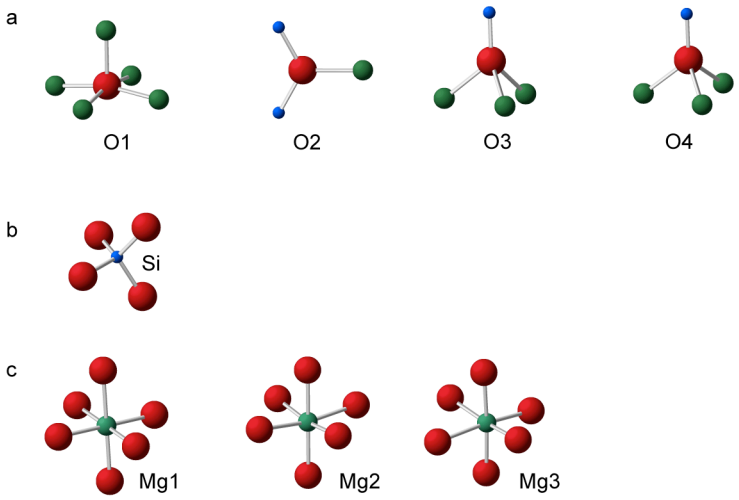

Figure S3.1 Local coordination environments for (a) oxygen, (b) silicon and (c) magnesium species taken from the crystal structure for anhydrous wadsleyite.[S1]

S4. Structural models used for DFT calculations

The six fully-hydrated ordered model structures were constructed by removing magnesium cations from the anhydrous wadsleyite crystal structure[S1] and manually inserting protons around the resulting vacancies. Full geometry optimisations were then performed, resulting in structures that closely resemble those identified in a recent DFT study by Tsuchiya *et al.*[S2] Optimised structures containing Mg2 vacancies are shown in Figure S4.1.

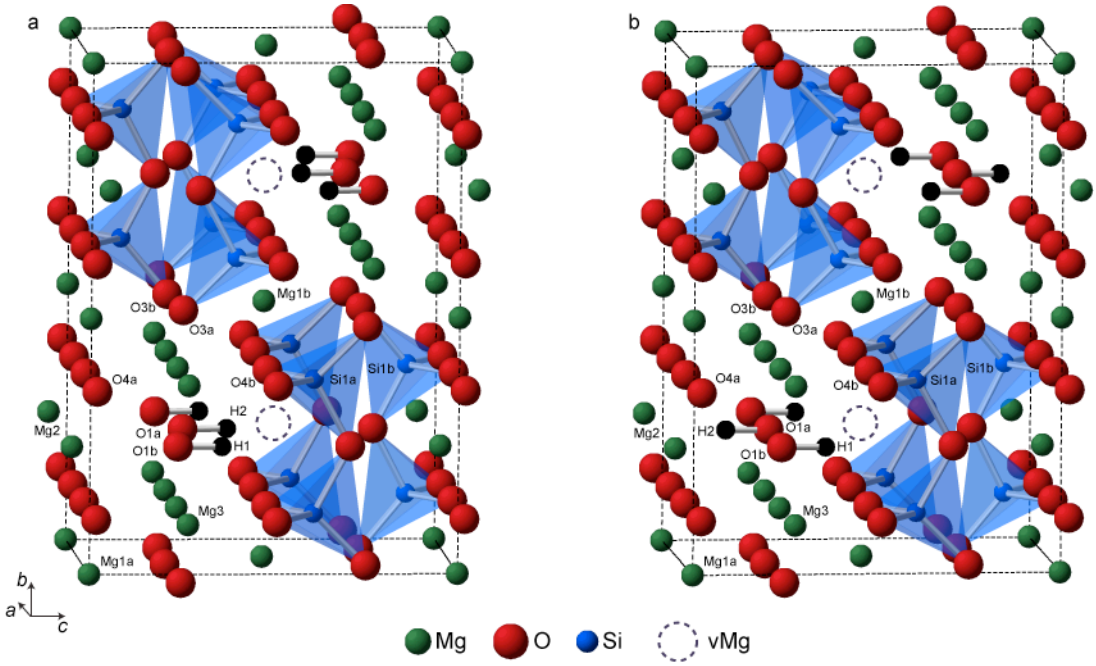

Figure S4.1 Fully-hydrated ordered model structures (a) vMg2^{a} and (b) vMg2^{b}, which contain cation vacancies on the Mg2 site. Crystallographically-distinct oxygen, magnesium and silicon sites are indicated for one half of the unit cell.

Optimised structures containing Mg3 vacancies are shown in Figure S4.2. The four structures differ in the ordering of the Mg3 vacancies in the two halves of the unit cell.

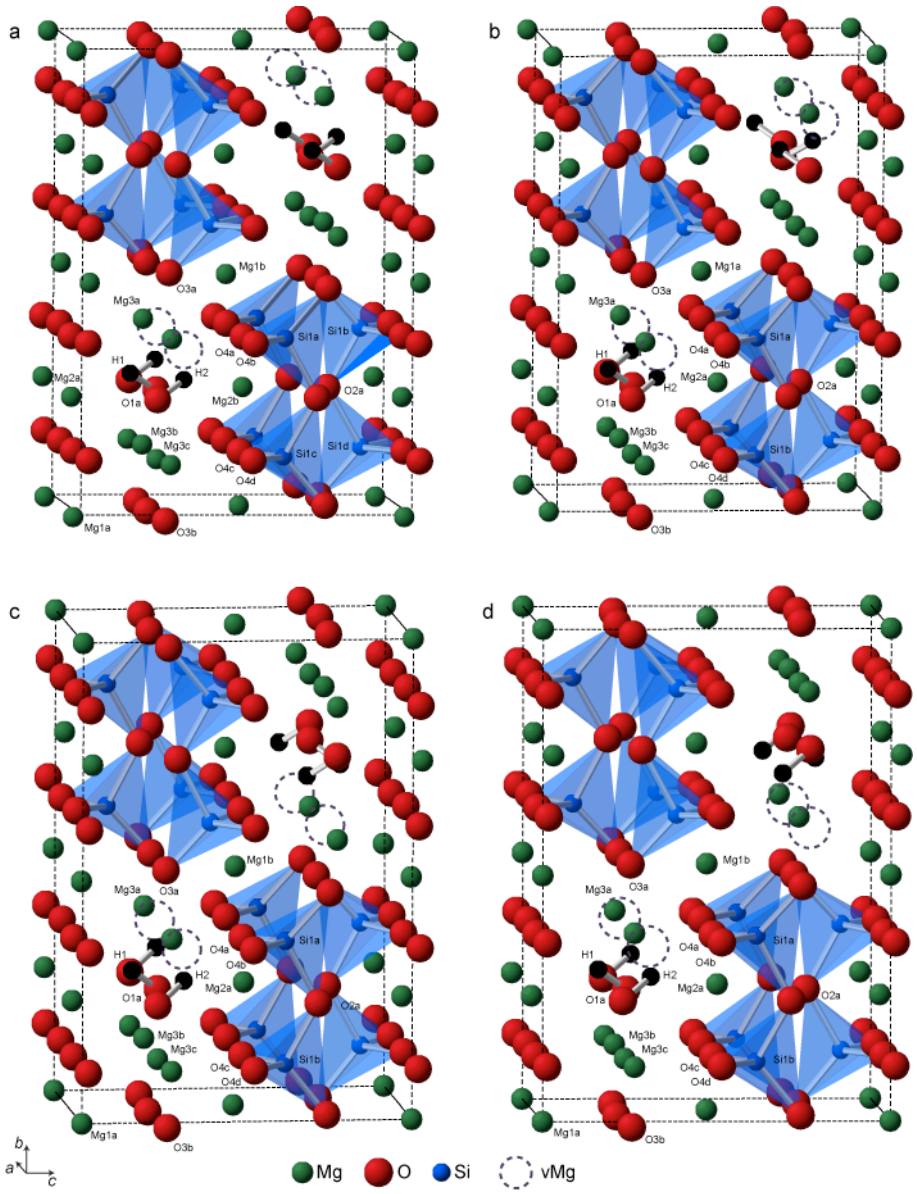

Figure S4.2 Fully-hydrated ordered model structures (a) vMg3^{a}, (b) vMg3^{b}, (c) vMg3^{c} and (d) vMg3^{d}, which contain cation vacancies on the Mg2 site.

Model structures containing alternative hydrated defects were based on a 2 × 1 × 1 supercell of the vMg3^{a} structure. The alternative defect was introduced into the structure either by replacing one of the hydrated Mg3 vacancies with a hydrated vacancy in another location (for alternative vacancies on the Mg1 and Mg2 sites), or by changing the proton configuration within one of the Mg3 vacancies. Model structures containing alternative vacancies on the Mg1 site are shown in Figure S4.3.

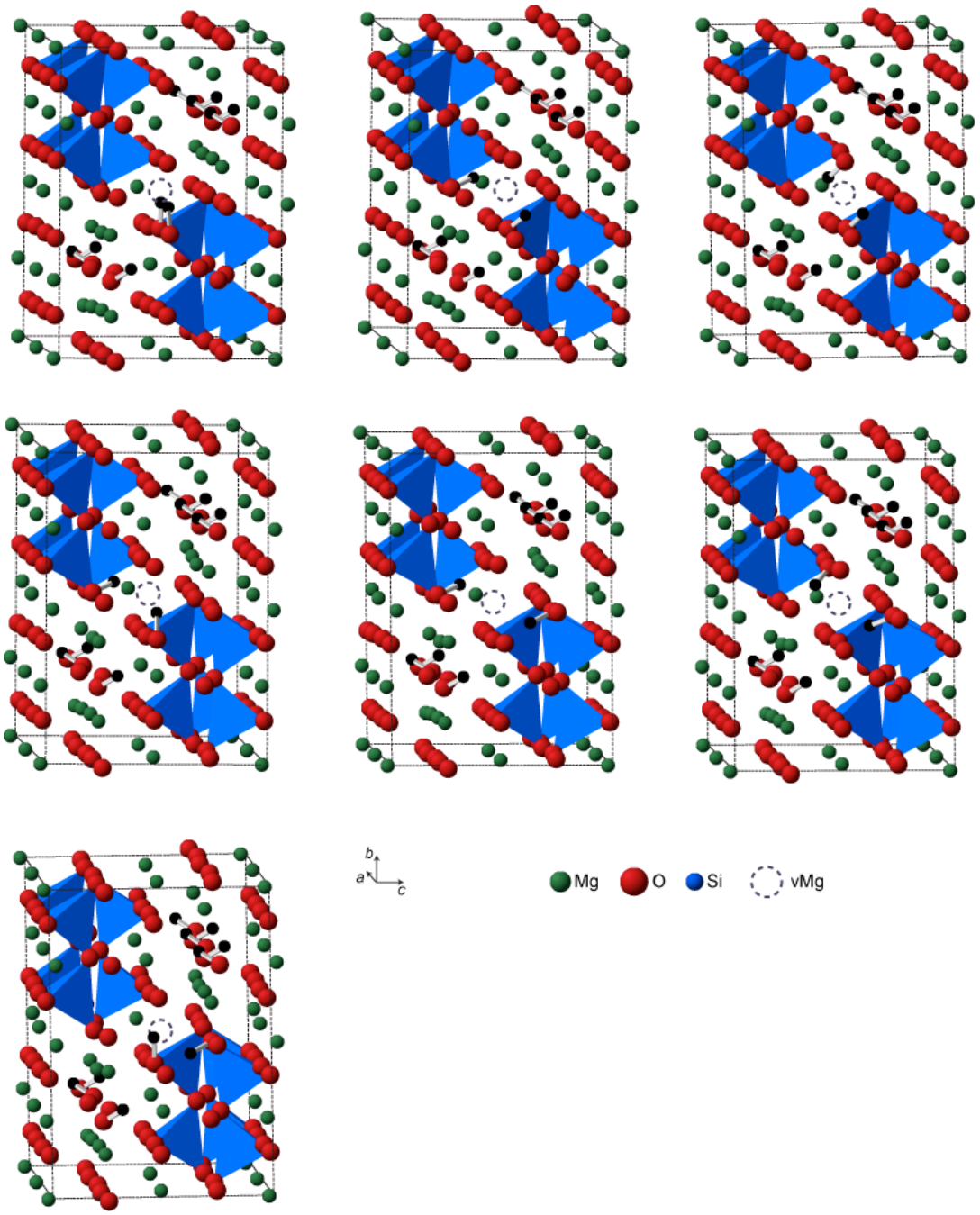

Figure S4.3 Model structures based on a 2 × 1 × 1 supercell of vMg3[a], with one of the hydrated Mg3 cation vacancies replaced with a hydrated cation vacancy on the Mg1 site.

Model structures containing alternative vacancies on the Mg2 site are shown in Figure S4.4.

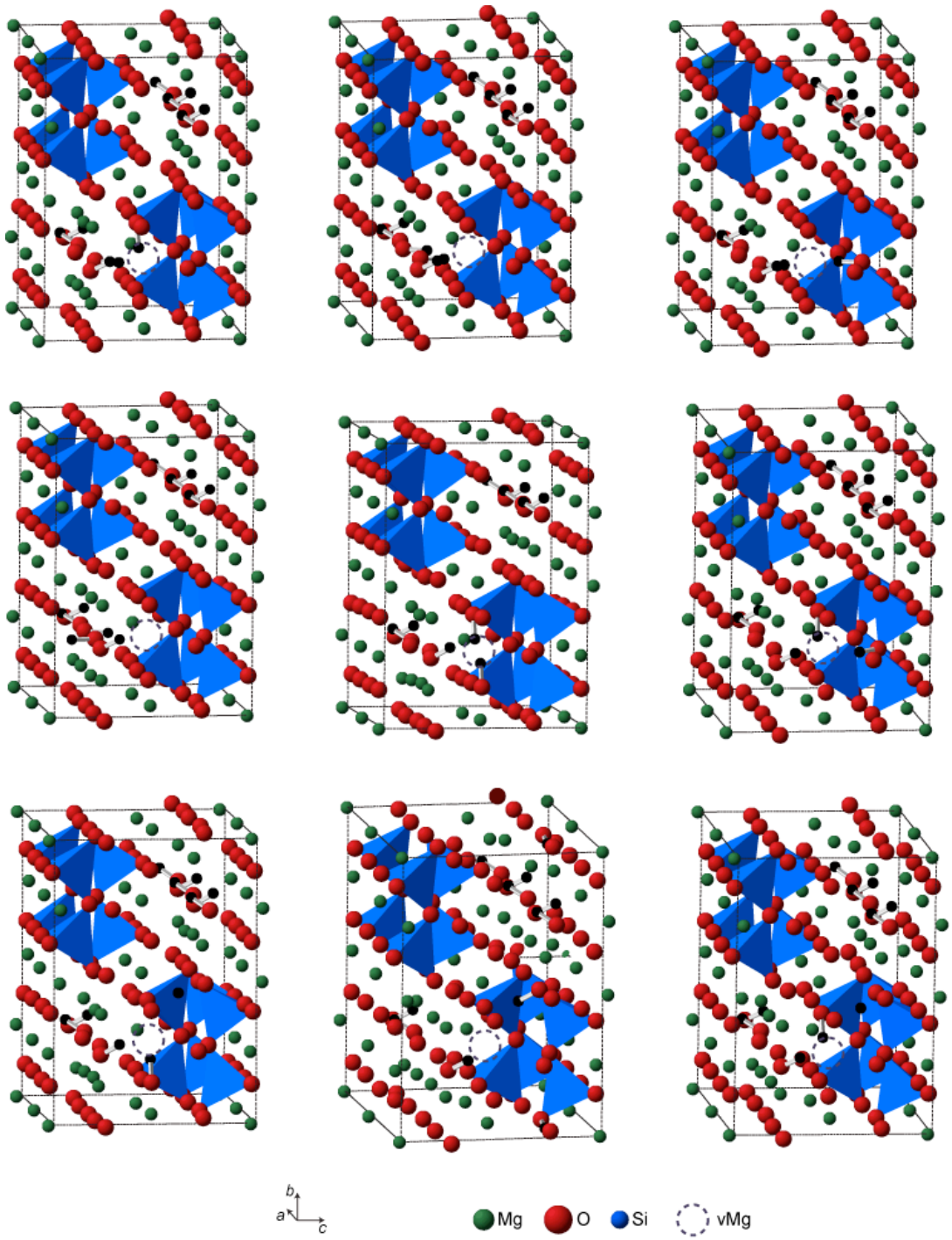

Figure S4.4 Model structures based on a 2 × 1 × 1 supercell of vMg3[a], with one of the hydrated Mg3 cation vacancies replaced with a hydrated cation vacancy on the Mg2 site.

Model structures with an alternative proton configuration within one of the hydrated Mg3 cation vacancies are shown in Figure S4.5.

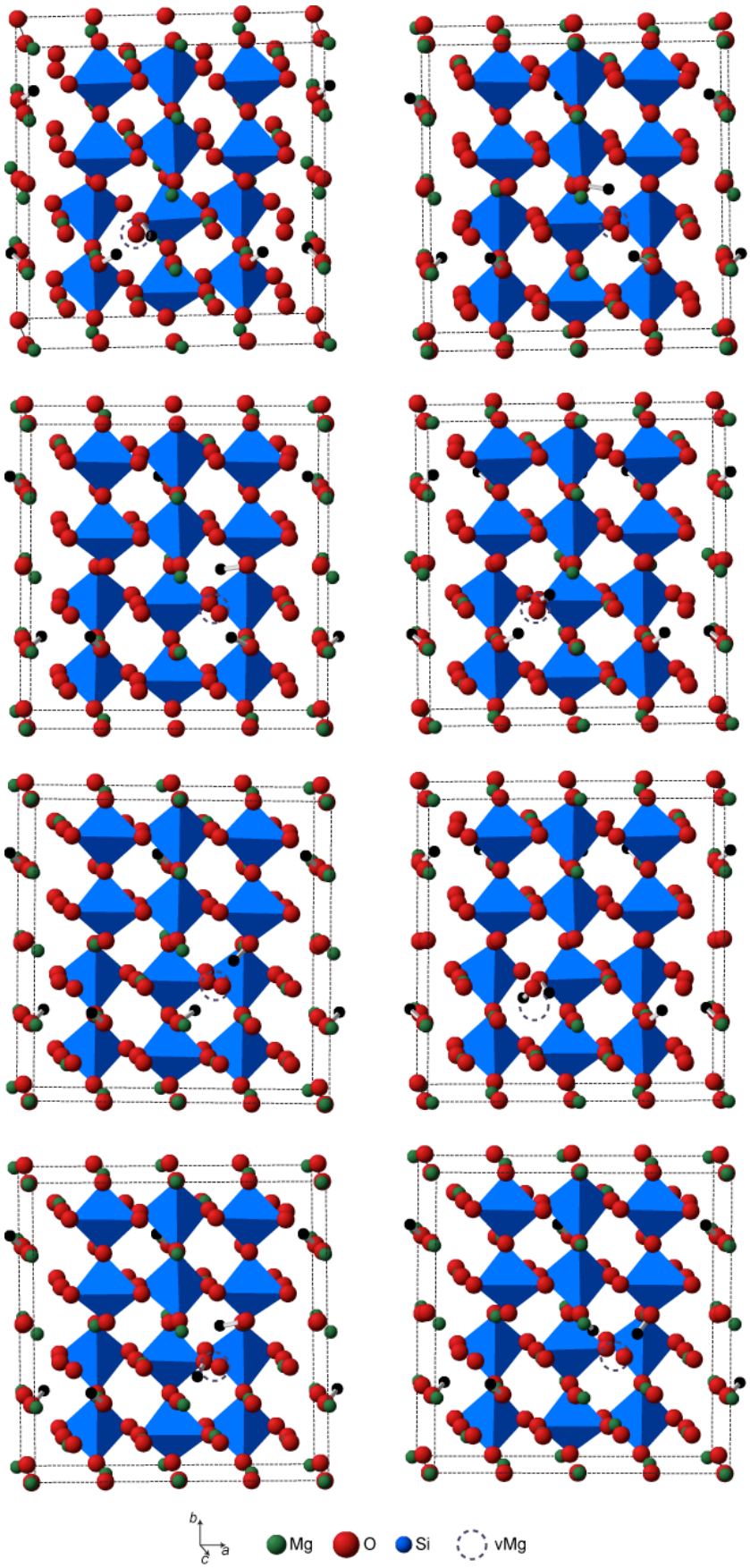

Figure S4.5 Model structures based on a 2 × 1 × 1 supercell of vMg3[a], with an alternative proton configuration in one of the hydrated Mg3 cation vacancies.

S5. Calculated ^{17}O and ^{25}Mg NMR parameters for fully-hydrated ordered model structures

Calculated ^{17}O NMR parameters for the fully-hydrated ordered model structures vMg2[a] and vMg2[b] are summarised in Table S5.1. For each structure, there are eight crystallographically-distinct oxygen sites owing to the lowering of the symmetry upon the incorporation of hydrogen into the structure.

Table S5.1 Calculated ^{17}O NMR quadrupolar coupling constants (C_Q^{calc}), asymmetry parameters (η_Q^{calc}) and isotropic chemical shifts (δ_{iso}^{calc}) for fully-hydrated ordered model structures vMg2[a] and vMg2[b].

	vMg2[a]			vMg2[b]		
Site	C_Q^{calc} / MHz	η_Q^{calc}	δ_{iso}^{calc} (ppm)	C_Q^{calc} / MHz	η_Q^{calc}	δ_{iso}^{calc} (ppm)
O1a	5.83	0.38	19.7	6.40	0.29	35.3
O1b	6.74	0.28	28.5	6.70	0.30	28.6
O2a	5.25	0.94	74.0	5.27	0.92	75.2
O2b	5.30	0.43	81.5	5.45	0.42	91.7
O3a	4.87	0.08	56.3	4.85	0.05	54.6
O3b	4.94	0.03	62.1	4.93	0.03	62.3
O4a	4.38	0.32	64.2	4.40	0.27	74.8
O4b	4.20	0.53	87.5	4.23	0.61	84.9

Calculated ^{17}O NMR parameters for the fully-hydrated ordered model structures vMg3^{a-d} are summarised in Table S5.2. For each structure, there are eight crystallographically-distinct oxygen sites owing to the lowering of the symmetry upon the incorporation of hydrogen into the structure.

Table S5.2. Calculated ^{17}O NMR quadrupolar coupling constants (C_Q^{calc}), asymmetry parameters (η_Q^{calc}) and isotropic chemical shifts (δ_{iso}^{calc}) for fully-hydrated ordered model structures vMg3^{a-d}.

	vMg3^a			vMg3^b			vMg3^c			vMg3^d		
Site	C_Q^{calc} / MHz	η_Q^{calc}	δ_{iso}^{calc} (ppm)	C_Q^{calc} / MHz	η_Q^{calc}	δ_{iso}^{calc} (ppm)	C_Q^{calc} / MHz	η_Q^{calc}	δ_{iso}^{calc} (ppm)	C_Q^{calc} / MHz	η_Q^{calc}	δ_{iso}^{calc} (ppm)
O1	6.84	0.30	16.6	7.13	0.35	15.2	7.08	0.32	14.4	6.80	0.30	16.4
O2	4.92	0.98	80.7	4.97	0.97	81.3	4.90	1.00	80.6	4.89	0.99	80.8
O3a	4.38	0.50	70.9	4.49	0.50	71.6	4.42	0.56	73.4	4.47	0.62	73.6
O3b	4.70	0.24	65.8	4.76	0.22	66.6	4.86	0.13	65.2	4.89	0.15	66.1
O4a	3.74	0.21	75.3	3.60	0.16	72.6	3.34	0.19	69.2	3.48	0.22	80.1
O4b	3.99	0.31	60.8	4.25	0.23	63.2	4.06	0.34	64.7	3.85	0.35	55.5
O4c	4.27	0.25	68.0	4.04	0.27	60.8	4.26	0.25	66.1	4.50	0.20	67.8
O4d	3.77	0.26	54.9	4.09	0.25	61.3	4.33	0.18	62.2	4.09	0.24	60.7

Calculated ^{25}Mg NMR parameters for anhydrous wadsleyite are summarised in Table S5.3.

Table S5.3. Calculated ^{25}Mg NMR quadrupolar coupling constants (C_Q^{calc}), asymmetry parameters (η_Q^{calc}) and isotropic chemical shifts (δ_{iso}^{calc}) for anhydrous wadsleyite.

	C_Q^{calc} / MHz	η_Q^{calc}	δ_{iso}^{calc} (ppm)
Mg1	8.08	0.35	20.5
Mg2	3.24	0.90	16.9
Mg3	5.20	0.74	24.5

Calculated ^{25}Mg NMR parameters for the fully-hydrated ordered model structures vMg2^a and vMg2^b are summarised in Table S5.4. For each structure, there are four crystallographically-distinct magnesium sites owing to the lowering of the symmetry upon the incorporation of hydrogen into the structure.

Table S5.4. Calculated ^{25}Mg NMR quadrupolar coupling constants (C_Q^{calc}), asymmetry parameters (η_Q^{calc}) and isotropic chemical shifts (δ_{iso}^{calc}) for fully-hydrated ordered model structures vMg2^a and vMg2^b.

	vMg2^a			vMg2^b		
Site	C_Q^{calc} / MHz	η_Q^{calc}	δ_{iso}^{calc} (ppm)	C_Q^{calc} / MHz	η_Q^{calc}	δ_{iso}^{calc} (ppm)
Mg1a	6.41	0.16	113.6	6.56	0.06	122.4
Mg1b	10.43	0.62	114.7	10.87	0.59	130.4
Mg2	3.47	0.73	112.6	3.29	0.66	99.2
Mg3	6.66	0.98	112.2	6.52	0.83	115.0

Calculated ^{25}Mg NMR parameters for the fully-hydrated ordered model structures vMg3^{a-d} are summarised in Table S5.5. For each structure, there are six crystallographically-distinct magnesium sites owing to the lowering of the symmetry upon the incorporation of hydrogen into the structure.

Table S5.5. Calculated ^{25}Mg NMR quadrupolar coupling constants (C_Q^{calc}), asymmetry parameters (η_Q^{calc}) and isotropic chemical shifts (δ_{iso}^{calc}) for fully-hydrated ordered model structures vMg3^{a-d}.

	vMg3^a			vMg3^b			vMg3^c			vMg3^d		
Site	C_Q^{calc} / MHz	η_Q^{calc}	δ_{iso}^{calc} (ppm)	C_Q^{calc} / MHz	η_Q^{calc}	δ_{iso}^{calc} (ppm)	C_Q^{calc} / MHz	η_Q^{calc}	δ_{iso}^{calc} (ppm)	C_Q^{calc} / MHz	η_Q^{calc}	δ_{iso}^{calc} (ppm)
Mg1a	8.21	0.15	112.6	6.91	0.58	105.0	7.43	0.24	124.7	8.37	0.42	130.4
Mg1b	8.21	0.15	109.4	-	-	-	-	-	-	-	-	-
Mg2a	4.47	0.76	106.6	5.38	0.80	98.7	5.92	0.52	112.4	7.31	0.59	115.6
Mg2b	4.48	0.76	106.2	-	-	-	-	-	-	-	-	-
Mg3a	5.72	0.34	110.9	6.18	0.40	101.4	3.52	0.83	108.4	4.45	0.79	105.7
Mg3b	4.76	0.02	119.0	4.93	0.20	130.1	7.08	0.60	125.4	6.26	0.22	130.1
Mg3c	5.13	0.21	116.6	4.57	0.18	109.5	4.28	0.21	132.2	3.78	0.30	124.2

S6. Calculation of total energies for hydrous wadsleyite model structures

For anhydrous wadsleyite, the unit cell contains eight formula units of Mg_2SiO_4. For hydrous wadsleyite, hydrogen incorporation is balanced by the removal of magnesium, with a maximum effective H_2O content of 3.3 wt%, corresponding to the removal of two magnesium cations per unit cell. The structure of wadsleyite can, therefore, be expressed as $Mg_{8-x}Si_4O_{16-2x}(OH)_{2x}$, where x can be 0 – 1, with the formula unit for fully-hydrated wadsleyite equal to $Mg_7Si_4O_{14}(OH)_2$. For the fully-hydrated ordered model structures vMg2[a,b] and vMg3[a-d] (shown in Figures S4.1 and S4.2), each unit cell contains two formula units of $Mg_7Si_4O_{14}(OH)_2$. For the alternative defect structures, which are based on a $2 \times 1 \times 1$ supercell of the basic wadsleyite structure, each unit cell contains four formula units of $Mg_7Si_4O_{14}(OH)_2$.

The first-principles GIPAW calculations yield total energies (E_{tot}) for each structure, expressed in eV. These values were converted to kJ mol^{-1} using the following relationship:

$$E_{tot}^{calc}\,(\text{kJ mol}^{-1}) = [\{ E_{tot}^{calc}\,(\text{eV}) \,/\, N_{FU} \} \times N_A \times e] \,/\, 1000 \qquad (1)$$

where N_{FU} is the number of formula units in the unit cell, N_A is Avogadro constant and e is the electronic charge. Total energies for each model structure considered in this work are summarised in Table S6.1.

Table S6.1 (overleaf) Calculated total energies, E_{tot}^{calc}, in eV and kJ mol^{-1} for the fully-hydrated ordered model structures and alternative defect structures considered in this work. Total energies relative to the lowest energy structure vMg3[a] (E_{tot}^{rel}) are also given.

Structure	E_{tot}^{calc} / eV	N_{FU}	E_{tot}^{calc} / kJ mol^{-1}	E_{rel}^{calc} / kJ mol^{-1}
vMg2[a]	–29942.34894596	2	–1443985.9	132.1
vMg2[b]	–29941.20206896	2	–1443930.6	187.5
vMg3[a]	–29945.08915284	2	–1444118.0	0.0
vMg3[b]	–29944.79053717	2	–1444103.6	14.4
vMg3[c]	–29944.40245220	2	–1444084.9	33.1
vMg3[d]	–29944.17315504	2	–1444073.8	44.2
defect Mg1[1]	–59889.19167369	4	–1444094.2	23.8
defect Mg1[2]	–59889.17155116	4	–1444093.7	24.3
defect Mg1[3]	–59889.15753519	4	–1444093.4	24.6
defect Mg1[4]	–59889.12976746	4	–1444092.7	25.3
defect Mg1[5]	–59889.06676136	4	–1444091.2	26.8
defect Mg1[6]	–59888.94719257	4	–1444088.3	29.7
defect Mg1[7]	–59888.94097690	4	–1444088.2	29.8
defect Mg2[1]	–59888.90002803	4	–1444087.2	30.8
defect Mg2[1]	–59888.88236099	4	–1444086.8	31.2
defect Mg2[3]	–59888.52836878	4	–1444078.2	39.8
defect Mg2[4]	–59888.37350575	4	–1444074.5	43.5
defect Mg2[5]	–59888.29100761	4	–1444072.5	45.5
defect Mg2[6]	–59887.46370344	4	–1444052.6	65.5
defect Mg2[7]	–59887.11600241	4	–1444044.2	73.8
defect Mg2[8]	–59886.88303527	4	–1444038.6	79.5
defect Mg2[9]	–59886.81501904	4	–1444036.9	81.1
defect Mg3[1]	–59889.41740120	4	–1444099.7	18.3
defect Mg3[2]	–59889.30937895	4	–1444097.1	21.0
defect Mg3[3]	–59889.26484164	4	–1444096.0	22.0
defect Mg3[4]	–59889.21796992	4	–1444094.9	23.2
defect Mg3[5]	–59889.21221898	4	–1444094.7	23.3
defect Mg3[6]	–59888.63715357	4	–1444080.9	37.2
defect Mg3[7]	–59888.42321284	4	–1444075.7	42.3
defect Mg3[8]	–59887.85879977	4	–1444062.1	55.9
defect Mg3[9]	–59889.41740120	4	–1444099.7	18.3

S7. ^{1}H MAS NMR spectrum and comparison of variable-temperature ^{2}H MAS NMR spectra for wads-D.

A ^{1}H MAS NMR spectrum of the residual protons in wads-D is shown in Figure S7.1(a). Rotor-synchronised ^{2}H MAS NMR spectra for wads-D obtained at temperatures of 298 and 373 K are shown in Figures S7.1(b) and (c). There is little change in the line widths of the resonances in the spectra over the temperature range investigated. This indicates that dynamic processes are not present within the sample.

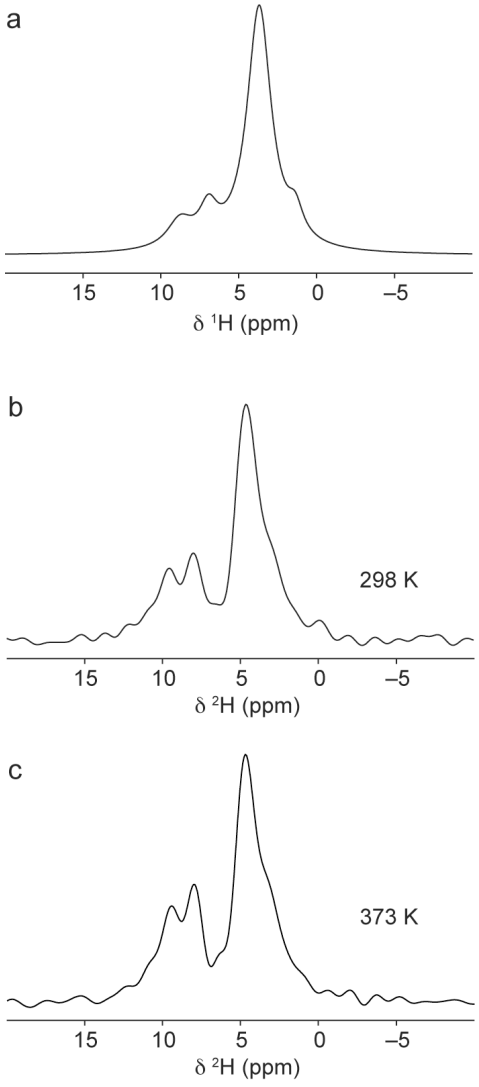

Figure S7.1 (a) ^{1}H (14.1 T) MAS NMR spectrum of wads-D. Rotor-synchronised ^{2}H (14.1 T) MAS NMR spectra recorded at temperatures of (a, b) 298 K and (b) 373 K. Spectra were recorded at MAS frequencies of (a) 30 kHz and (b, c) 12.5 kHz and are the result of averaging (a) 16, (b) 4126 and (c) 28984 transients separated by recycle intervals of (a) 2 s and (b, c) 5 s.

S8. ^{29}Si and ^{1}H solid-state NMR of superhydrous phase B

In recent work by Stebbins *et al.*,[S3] the observation of a resonance at –75 ppm in ^{29}Si CPMAS NMR spectra of hydrous wadsleyite was attributed to a phase B impurity. However, X-ray diffraction experiments on the samples studied in the current work showed no indication of a phase B impurity, or of the related superhydrous phase B. No sample of phase B was available for study, but as a further check for the presence of superhydrous phase B, a ^{29}Si CPMAS NMR experiment was performed on a separate mixed-phase sample known to contain this phase. The ^{29}Si CPMAS NMR spectrum of this sample, recorded with a contact time of 10 ms, is shown in Figure S8.1(a). The spectrum exhibits resonances at –74.8 ppm and –166.9 ppm, corresponding to the Si^{IV} and Si^{VI} sites in the crystal structure of superhydrous phase B.[S4] These values are in good agreement with those quoted by Phillips *et al.*[S5] in a previous ^{29}Si NMR study of high-pressure minerals. ^{29}Si CPMAS NMR spectra of wads-H recorded with contact times in the range 1 – 10 ms are shown in Figure S8.1(b). In these spectra, a resonance is also observed at approximately –74.8 ppm (as described in the main text). The relative intensity of this resonance is highest at short contact times, indicating that it corresponds to silicon species that are close to protons in the structure. However, at all contact times the Si^{VI} resonance that would be expected if superhydrous phase B were present is not observed within the signal-to-noise obtained in the experiment. This indicates that the resonance at –74.8 ppm in the hydrous wadsleyite spectra correspond to silicon species within the wadsleyite structure itself.

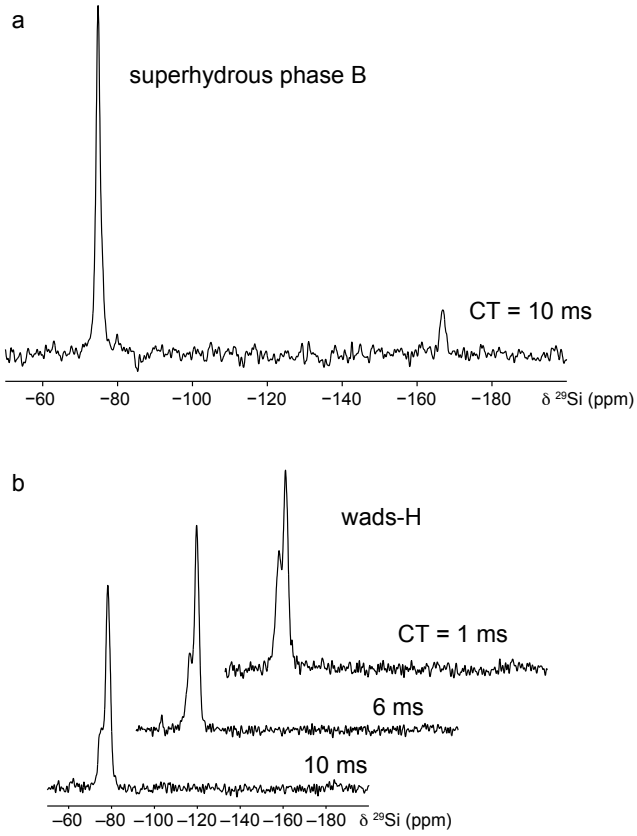

Figure S8.1 ^{29}Si (14.1 T) CPMAS NMR spectra of (a) superhydrous phase B and (b) wads-H. Spectra were recorded at a MAS frequency of 12.5 kHz and are result from averaging (a) 19480 and (b) between 2400 and 4800 transients separated by a recycle interval of 3 s.

A rotor-synchronised ^{1}H DQMAS NMR spectrum of superhydrous phase B is shown in Figure S8.2. In this spectrum, a DQ correlation between the two distinct OH protons in the structure is observed at δ_{DQ} = 4.2 + 3.2 = 7.4 ppm. This is in good agreement with a previous ^{1}H NMR study of superhydrous phase B.[S6] Another autocorrelation is also observed at δ_{DQ} = 2.4 ppm; this resonance does not correlate with the other resonances in the spectrum, indicating that it corresponds to another phase present in the sample, or is a background signal from the rotor. Importantly, no resonances are observed at chemical shifts greater than 6 ppm. This confirms that the ^{1}H resonances at high chemical shift observed in the ^{1}H NMR spectrum of wads-H correspond to protons within the hydrous wadsleyite structure and do not result from a superhydrous phase B impurity.

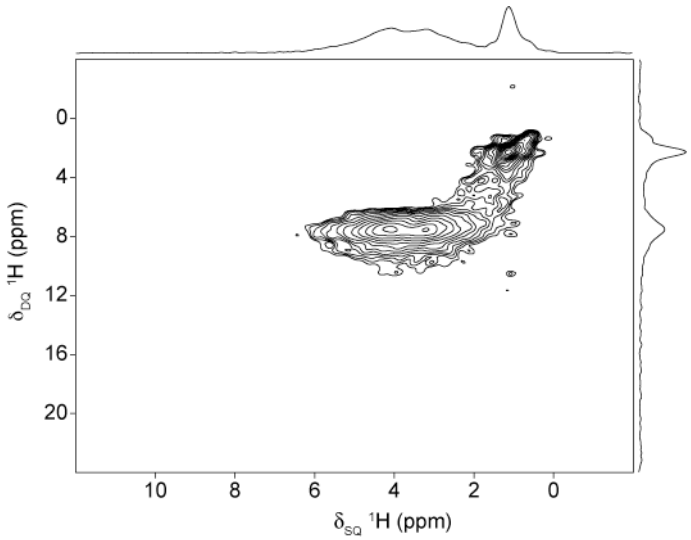

Figure S8.2 A rotor-synchronised ^{1}H (14.1 T) DQMAS NMR spectrum of superhydrous phase B recorded at a MAS frequency of 30 kHz. The spectrum is the result of averaging 32 transients for each of the 128 t_1 increments of 33.33 µs. The recycle interval was 3 s.

S9. References

S1. Horiuchi, H.; Sawamoto, H. *Am. Mineral.* **1981**, *66*, 658.

S2. Tsuchiya, J.; Tsuchiya, T. *J. Geophys. Res.* **2009**, *114*, B02206.

S3. Stebbins, J. F.; Smyth, J. R.; Panero, W. R.; Frost, D. J. *Am. Mineral.* **2009**, *94*, 905.

S4. Koch-Müller, M.; Dera, P.; Fei, Y.; Hellwig, H.; Liu, Z.; van Orman, J.; Wirth, R. *Phys. Chem. Min.* **2005**, *32*, 349.

S5. Phillips, B. L.; Burnley, P. C.; Worminghaus, K.; Navrotsky, A. *Phys. Chem. Min.* **1997**, *24*, 179.

S6. Xue, X.; Kanzaki, M.; Shatskiy, A. *Am. Mineral.* **2008**, *93*, 1099.